FRONTIER LETTER

Open Access

Design and operation of a 1500-m laser strainmeter installed at an underground site in Kamioka, Japan

Akito Araya[1*], Akiteru Takamori[1], Wataru Morii[2], Kouseki Miyo[3], Masatake Ohashi[3], Kazuhiro Hayama[3], Takashi Uchiyama[3], Shinji Miyoki[3] and Yoshio Saito[3]

Abstract

A laser strainmeter with a 1500-m baseline was constructed at an underground site in Kamioka, Gifu Prefecture, Japan, and has been operating since August 2016. The laser interferometer measures the change in distance between two retroreflectors housed in two vacuum chambers with a separation of 1500 m. The retroreflectors are fixed to the ground in the tunnel of the KAGRA gravitational wave telescope. A high-frequency-stabilized laser is used as a light source; it achieves an Allan variance of 3×10^{-13}. Since operations began, ground motions with large amplitude and timescale variations have been detected. The recorded tidal waveform almost agrees with the theoretical waveform; however, a slight difference of ~13% in amplitude is found, likely due to a topographic effect. The strain spectrum of the observed data for the 1500-m strainmeter indicates that the lowest background noise attained is less than 10^{-12} in the mHz band. Seismic waves up to 6×10^{-7} in amplitude have been observed without saturation or fringe steps. The strainmeter, with its excellent resolution, dynamic range, and bandwidth performance, provides a new method for observing low-frequency ground motion on seismic, geodetic, and intermediate timescales.

Keywords: Laser, Interferometer, Strainmeter, Kamioka, KAGRA, Earth tide

Introduction

Ground motions are measured using various methods depending on the spatial scale and frequency range. For large ground motions, the global navigation satellite system (GNSS) is commonly used to measure ground motions with amplitudes of more than ~1 mm at frequencies below ~10 Hz. In contrast, strong-motion seismometers cover accelerations of ~10^{-4} to 40 m/s^2 at frequencies <30 Hz. For small ground motion, short-period or broadband seismometers are suitable for the high-frequency range, with accelerations of ~10^{-9} to 10^{-3} m/s^2 in the frequency range of 3 mHz–100 Hz. However, their sensitivity is limited at low frequencies due to the short resonant period of the reference pendulum.

Strainmeters can measure low-frequency ground motion at high resolution either with a mechanical reference to a low-expansion rod or wire (Benioff 1959; Mentes 2010; Zürn et al. 2015) or with an optical reference to a laser wavelength (Vali et al. 1965; Vali and Bostrom 1968; Berger and Lovberg 1970; Agnew 1986; Crescentini and Renzella 1991; Buklerskii et al. 1995; Araya et al. 2002; Takemoto et al. 2004; Park et al. 2008). The performance of mechanical strainmeters is essentially limited by reference problems, due to such physical parameters as thermal expansion and nonlinearities in rods or wires. Laser strainmeters solve these problems by replacing the reference with a highly stabilized optical wavelength. Nevertheless, laser strainmeters are still affected by local site characteristics. For example, the 100-m laser strainmeter in Kamioka, Japan, is capable of measuring small coseismic strain steps originating from distant earthquakes even following strong motion from seismic waves (Araya et al. 2010). However, this laser strainmeter can be affected by ground water on longer

*Correspondence: araya@eri.u-tokyo.ac.jp
[1] Earthquake Research Institute, University of Tokyo, 1-1-1 Yayoi, Bunkyo-ku, Tokyo 113-0032, Japan
Full list of author information is available at the end of the article

Araya *et al. Earth, Planets and Space* (2017) 69:77

Page 2 of 7

timescales (Araya et al. 2007). Such local effects might be mitigated using a long-baseline strainmeter.

A 1500-m laser strainmeter, the longest laser interferometer for geophysical observations to our knowledge, was constructed at an underground site at Kamioka, Gifu Prefecture, Japan. In addition to the 100-m-scale interferometers, km-scale interferometers, especially geophysical strainmeters requiring broadband and a wide dynamic range, need to be carefully designed for optics and signal detection. In this study, after describing the laser strainmeter design and operation, observation data and instrument performance estimated from the data are discussed.

The 1500-m laser strainmeter

The location of the laser strainmeter is shown in Fig. 1. The site is part of the tunnel housing the KAGRA gravitational wave telescope (Somiya 2012) and is located below the cosmic-ray research facilities Super Kamiokande, KamLAND, CLIO, and XMASS (Fukuda et al. 2003; Araki et al. 2005; Miyoki et al. 2006; Abe et al. 2013). The measuring orientation of the strainmeter is N60°E, horizontal, and it is nearly parallel to the Atotsugawa

fault, which is approximately 0.5 km from the instrument (Ohzono et al. 2011). The depth of the tunnel from the surface is more than 200 m at the location of the laser strainmeter. The temperature of the site is stable at approximately 11.4 ± 0.1 °C without any diurnal change. Two vacuum chambers with a diameter of 1.1 m and a height of 1.0 m are mounted on granite blocks, which rest on a smoothly polished bedrock surface. Cement is cast around the granite blocks to fix them. The thicknesses of the granite blocks are 650 and 945 mm, depending on the depth of bedrock below the floor, and the granite blocks are separated from the floor by grooves. The separation of the chambers is 1500 m, and they are connected with vacuum pipes. Bellows are inserted between the pipes and chambers to reduce any disturbance from the pipes. The parameters related to the configuration of the strainmeter and optics are summarized in Tables 1 and 2, respectively.

The optical layout of the 1500-m laser strainmeter is shown in Fig. 2. Two retroreflectors, each housed in a chamber, and a beam splitter form an asymmetric Michelson interferometer. The long measurement arm, formed between both vacuum chambers with a
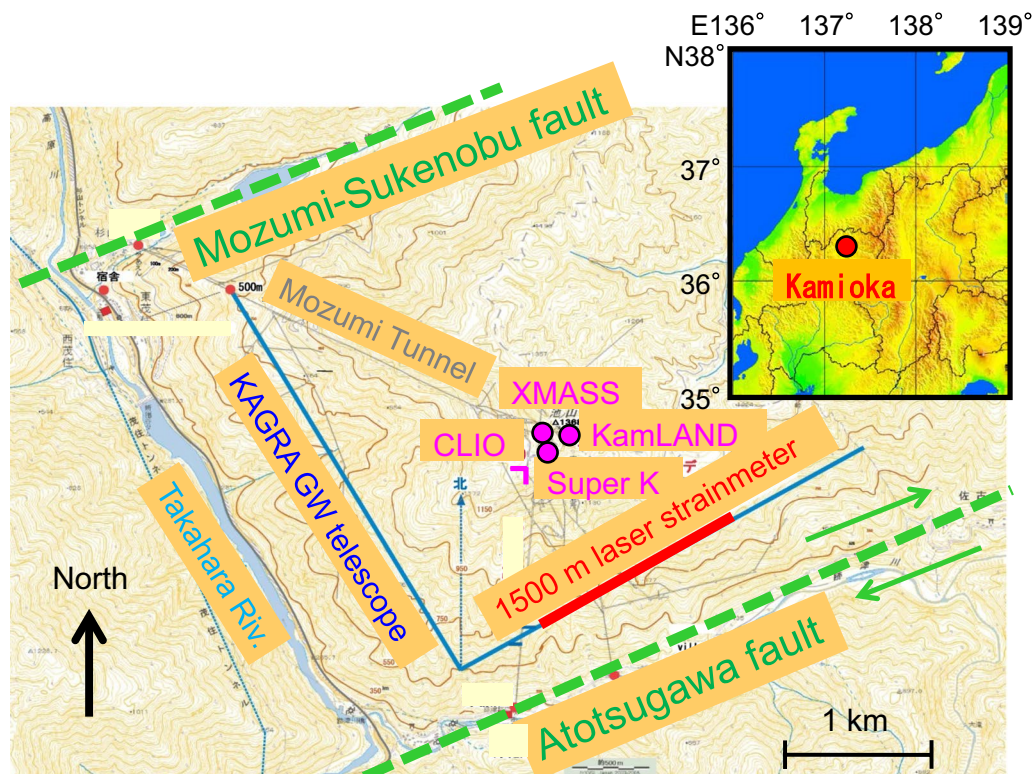
Fig. 1 Location of the 1500-m laser strainmeter and other facilities at the Kamioka underground site. The Atotsugawa fault is located approximately 0.5 km from the strainmeter and is almost parallel. This figure is modified from a map released by the Geospatial Information Authority of Japan (GSI)

Araya *et al. Earth, Planets and Space* (2017) 69:77

Page 3 of 7

Table 1 Configuration parameters of the 1500-m laser strainmeter

Item	Value
Coordinates	36°25′48″N, 137°18′36″E
Altitude above sea level	358 m
Depth below the surface	>200 m
Orientation	N60°E, horizontal
Baseline length	1500 m
Diameter of vacuum pipes	400 mm
Designed average pressure in vacuum pipes	<0.01 Pa

Table 2 Optical parameters for the 1500-m laser strainmeter
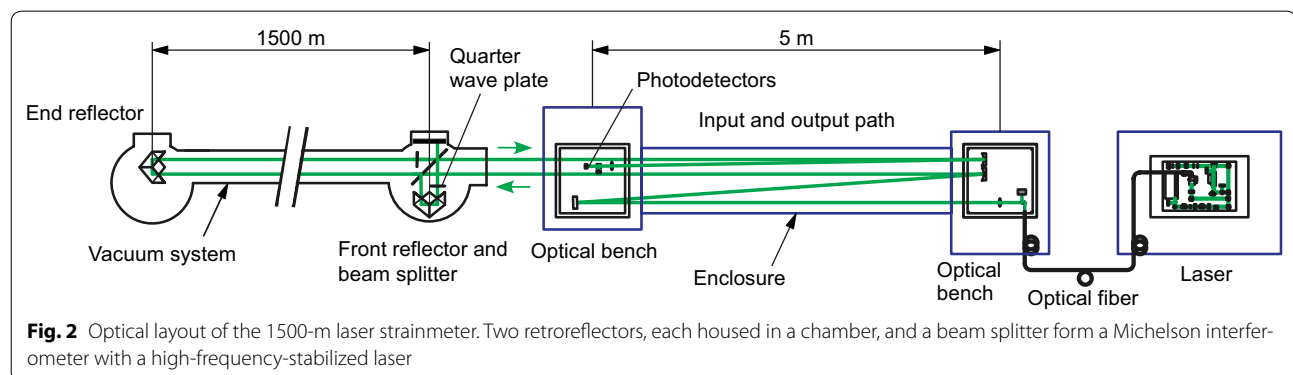
Item	Value
Laser (wavelength)	Frequency-doubled Nd:YAG (532 nm)
Estimated frequency stability	3×10^{-13} (Allan variance estimation)
Beam diameter	
Front	45 mm
End	32 mm
Retroreflector	
Aperture diameter	380 mm
Flatness	0.2 μm
Parallelism	2 μrad

1500-m baseline, responds to the ground motion. The short reference arm, formed within the front chamber with a 0.5-m baseline, is fixed on a plate made of super invar, which has a low thermal expansion index. The plate is regarded as the constant baseline. All interferometer optical paths are maintained in a vacuum. The optical path length (L_{opt}) of the baseline (L) is given by $L_{opt} = nL$, where n is the average refractive index of the optical path relative to the path in the vacuum. Index n is approximated as $n = 1 + c_0 p/p_0$, where $1 + c_0$, p_0, and p are the relative refractive index, pressure in standard air (at 1 atm), and vacuum pressure, respectively. The apparent strain due to the vacuum pressure is approximated using $\Delta\varepsilon = (L_{opt} - L)/L = c_0 p/p_0 \sim 3 \times 10^{-9}\, p$ (Pa) (Ciddor 1996). To attain the designed strain sensitivity (3×10^{-13}), the vacuum is required to remain below 1×10^{-4} Pa. By considering the attainable pressure in the current vacuum system and actual background strain, the average pressure in the pipes is designed to remain below 0.01 Pa, as listed in Table 1, and the measured pressure is used to correct the strain to attain actual strain sensitivity $\Delta\varepsilon \sim 10^{-12}$.

The laser beam is introduced into the vacuum chamber through an optical window after it has been collimated in the input path with optical benches at 5-m separation. To avoid aberrations in the expansion optics, the beam diameter is gradually expanded to ~100 times from the output of the optical fiber. The beam diameter of the interferometer needs to be large enough to prevent degrading due to a mismatch in interference beams during the 3-km round-trip. Furthermore, it needs to allow confinement in the vacuum pipes because the beam diameter (d) at wavelength (λ) and distance (z) from the beam waist position is approximately inversely proportional to the beam waist size (diameter d_0), given as $d = d_0\sqrt{1 + (4\lambda z)^2/(\pi^2 d_0^4)} \sim 4\lambda z/(\pi d_0)$ for a Gaussian beam, where $z \gg d_0^2/\lambda$ (Kogelnik and Li 1966). To minimize the diameter for the 3-km round-trip beam, the beam waist should be $d_0 = \sqrt{4\lambda L/\pi}$ and located at the end reflector. Then, the beam diameter of the front reflector is minimized to $\sqrt{2}d_0$. Accordingly, the retroreflectors and beam splitter have a large aperture, more than ~3d, to prevent chipping of the beam. Because the diameters of the vacuum pipes need to be much more than $6d = 270$ mm to confine the round-trip beams, we used 400 mm for the actual system. The optical parameters used for this design are listed in Table 2.

The light source is a frequency-doubled Nd:YAG laser emitting at an optical wavelength of $\lambda = 532$ nm. The laser frequency is stabilized with reference to an

Fig. 2 Optical layout of the 1500-m laser strainmeter. Two retroreflectors, each housed in a chamber, and a beam splitter form a Michelson interferometer with a high-frequency-stabilized laser

Araya *et al. Earth, Planets and Space* (2017) 69:77

Page 4 of 7

iodine-saturated absorption spectrum and attains an Allan variance of 3×10^{-13} as the lowest relative frequency stability (Araya et al. 2002). The stabilized laser beam is introduced into the input path through a polarization-maintaining optical fiber. The interference fringes are detected using two photodetectors on the input optical bench. A quadrature detection technique, as shown in Fig. 3, is used. Using a quarter-wave plate inserted in the reference arm of the interferometer, the optical phase is shifted by $\pi/2$ between the horizontal and vertical polarizations, and thus, quadrature fringe signals are obtained for both polarizations. The Lissajous curve produced from the two complementary fringe signals allows bidirectional detection of the mirror motion. The displacement resolution depends on both the wavelength and its detectable fraction, as in ordinary interferometers. However, the measurement range is arbitrarily wide because the fringes are periodic, unless they are lost due to misalignment or a low sampling rate. The fringe signals are sampled using 24-bit analog-to-digital converters (ADCs, PXI-5922, National Instruments Corp.) located onsite with a sampling rate of 50 kHz, which is synchronized with a rubidium atomic clock. The recorded data can be accessed from outside the tunnel and downloaded every minute to a storage device outside the mine, and the stored data are converted to strain automatically as follows.

The Lissajous curve is fitted to an ellipse (Heydemann 1981; Zumberge et al. 2004) and normalized to a unit circle to obtain the optical phase, φ, which is proportional to the change in the interferometer arm length, ΔL,

$$\varphi = \frac{4\pi}{\lambda} \Delta L. \tag{1}$$

Therefore, the strain, ε, can be obtained from the formula

$$\varepsilon = \frac{\Delta L}{L} = \frac{\lambda}{4\pi L} \varphi, \tag{2}$$

where L is the baseline length of 1500 m. The raw strain data (50 kHz samples) are filtered and averaged to produce 5 kHz, 200 Hz, or 20 Hz data. These data are stored and used for maintenance, seismic, and geodetic analyses.
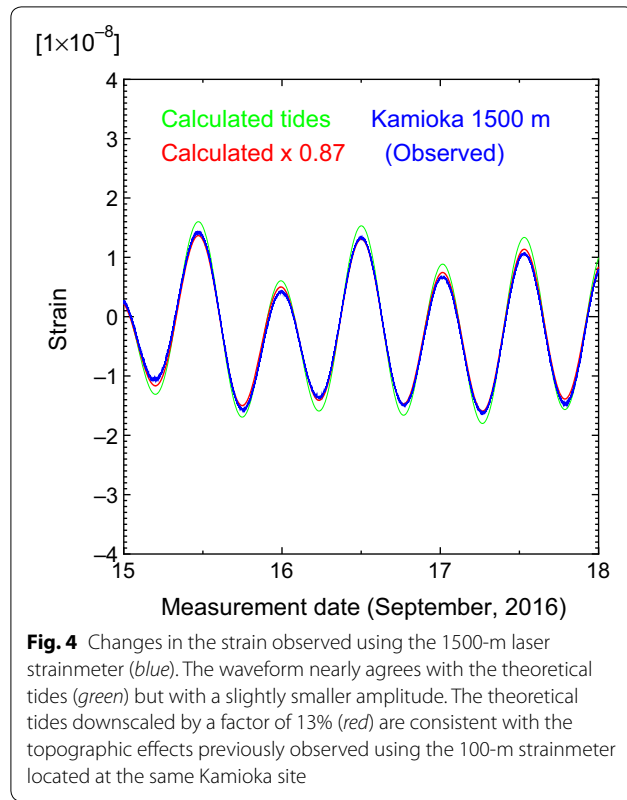
Results and discussion

In Fig. 4, a typical strain change observed by the 1500-m laser strainmeter (blue) is shown together with the theoretical tidal change (green) calculated with the tidal calculation program GOTIC2 (Matsumoto et al. 2001), including both solid and ocean tides. The waveforms are in good agreement with each other; however, a slight difference in amplitudes can be seen. An approximately 13% reduction in the theoretical amplitude (red) fits the
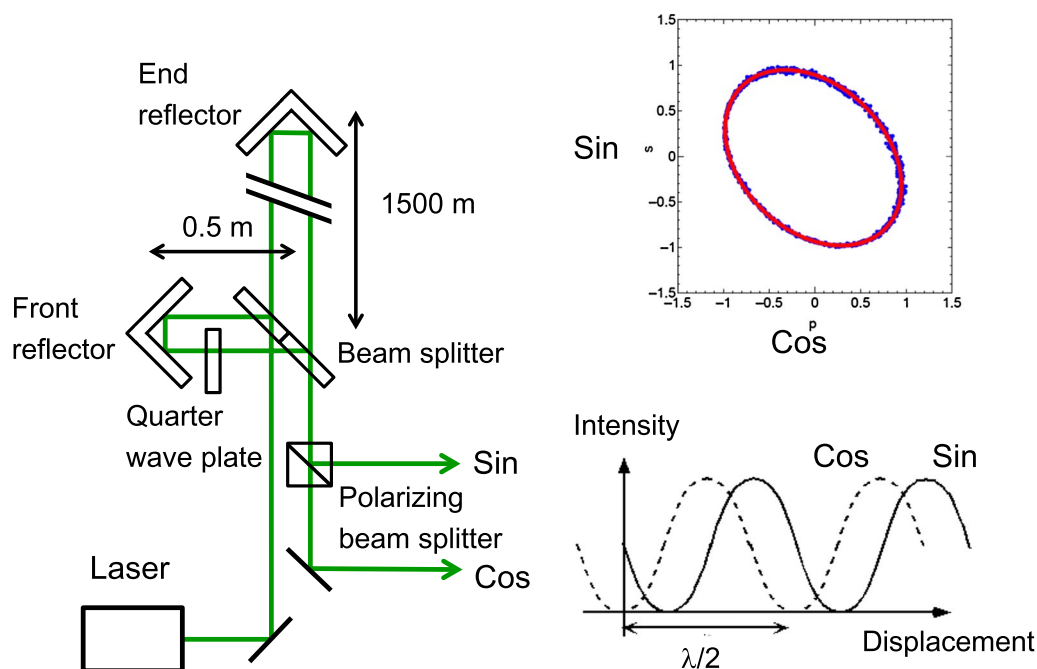
Fig. 3 Quadrature interferometer used in the 1500-m laser strainmeter (*left*). A quarter-wave plate inserted in the interferometer produces a 90° phase shift between the horizontal and vertical polarizations. As a result, the intensities of the interference beams for both polarizations separated by the polarizing beam splitter complementarily change as sine and cosine (*bottom right*). By normalizing the observed elliptic Lissajous curve (*top right*) into a circular one, mirror motion can be determined from the phase angle

Araya *et al. Earth, Planets and Space* (2017) 69:77

Page 5 of 7

Fig. 4 Changes in the strain observed using the 1500-m laser strainmeter (*blue*). The waveform nearly agrees with the theoretical tides (*green*) but with a slightly smaller amplitude. The theoretical tides downscaled by a factor of 13% (*red*) are consistent with the topographic effects previously observed using the 100-m strainmeter located at the same Kamioka site

Fig. 5 Background strain spectrum for the 1500-m laser strainmeter (*red*) compared to those for other strainmeters: Piñon Flat Observatory (PFO, *black*, Berger and Lovberg 1970; Berger and Levine 1974), Baksan (*pink*, Buklerskii et al. 1995), Gran Sasso (*gray*, Crescentini and Renzella 1991), Inuyama (*green*, Araya et al. 2001), and Black Forest Observatory (BFO, *orange*, Zürn et al. 2015), including the 100-m laser strainmeter at Kamioka (*blue*, Araya et al. 2007). Detectable strain levels in amplitude are shown as *dash-dotted lines*. The detection limit for the 1500-m strainmeter is estimated as better than 10^{-12} in the 2–20 mHz range and 10^{-11} in the 1 mHz–10 Hz range

observations. The reduction ratio is consistent with the topographic effects at the underground site, as observed from the 100-m strainmeter at Kamioka (Takemoto et al. 2004, 2006).

The background strain spectrum obtained using the 1500-m laser strainmeter (red) together with those for other strainmeters is shown in Fig. 5. A fast Fourier transform is applied to the 20 Hz strain data (32,768 data points) to obtain the frequency spectra with an applied Hanning window. The figure shows the square root of the power spectral density ($\tilde{\varepsilon}$) in units of $1/\sqrt{\text{Hz}}$. The dash-dotted lines indicate the estimated detectable strain based on the root-mean-square amplitude (ε_{RMS}) under the assumption

$$\tilde{\varepsilon} \sim \frac{\varepsilon_{\text{RMS}}}{\sqrt{f}}, \tag{3}$$

where f is the frequency. The detection limit for the 1500-m strainmeter is estimated as better than 10^{-12} in the 2–20 mHz range and 10^{-11} in the 1 mHz–10 Hz range. Compared to the 100-m strainmeter in Kamioka, the 1500-m strainmeter has a lower background noise in the 1–20 mHz range. Both strainmeters have nearly identical laser stabilization systems, and the reduction in background noise in this frequency range indicates the
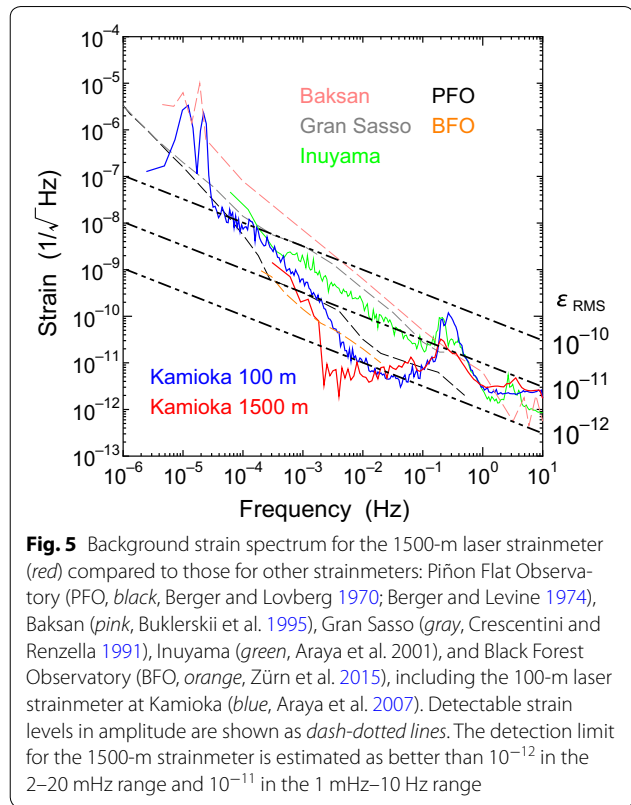
effects of spatial averaging for the long-baseline strainmeter. The noise level rapidly increases below 2 mHz and is larger than that found at the Black Forest Observatory (BFO) below ~1.5 mHz. According to Zürn et al. (2015), the barometric pressure affects the background strain in this frequency range, and therefore, the observed noise is inferred to be the ground response to air pressure changes.

Conversely, the response of the long-baseline strainmeter to seismic waves diminishes at high frequencies. It is assumed that sinusoidal plane seismic waves with a displacement amplitude of $\vec{u_0} = (u_{0x}, u_{0y}, u_{0z})$, angular frequency of $\omega = 2\pi f$, and wavenumber vector of $\vec{k} = (k_x, k_y, k_z)$ are incident on the laser strainmeter with baseline L and orientation $\vec{n}_x = (1, 0, 0)$. Then, the change in mirror separation detected by the laser interferometer can be expressed as

$$\Delta L = u_{0x} \sin(\omega t) - u_{0x} \sin(\omega t - k_x L)$$
$$= 2u_{0x} \sin\left(\frac{k_x L}{2}\right) \cos\left(\omega t - \frac{k_x L}{2}\right). \tag{4}$$

Because the waves generate strain amplitude of $u_{0x}k_x$, the response of the laser strainmeter ($H(f)$) to the seismic strain is given by:

Araya *et al. Earth, Planets and Space* (2017) 69:77

Page 6 of 7

$$H(f) = \frac{\Delta L}{u_{0x}k_xL} = 2\sin\left(\frac{k_xL}{2}\right)\Big/(k_xL) \sim 1 - \frac{1}{6}\left(\frac{k_xL}{2}\right)^2$$

$$= 1 - \frac{1}{6}\left(\frac{\pi L}{v_x}\right)^2 f^2, \tag{5}$$

where v_x is the apparent velocity in the x-direction. The corresponding cutoff frequency for the strain response is

$$f_c = \frac{\sqrt{3}}{\pi}\frac{v_x}{L}. \tag{6}$$

Assuming $v_x = 5$ km/s, f_c is 1.8 Hz for the 1500-m strainmeter. Therefore, it can respond to seismic strains below ~1 Hz. For this reason, the background noise above 1 Hz in Fig. 5 may not indicate the actual amplitude of the seismic strain.

The laser frequency stabilization is based on Araya et al. (2002). The square root of the Allan variance is approximated as $5 \times 10^{-13}/\sqrt{\tau}$ for a measurement time interval of $\tau < 20$ s from Figure 5 in Araya et al. (2002). White frequency noise with a constant power spectral density (h_0) has a dependency on $\sqrt{h_0/(2\tau)}$ in the square root of the Allan variance (Barnes et al. 1971), and laser frequency noise is estimated as $\sqrt{h_0} = 7 \times 10^{-13}/\sqrt{\text{Hz}}$ above ~0.05 Hz. The background strain noise in Fig. 5 above ~1 Hz is about three times the estimated frequency noise. However, the white nature and baseline independence, compared to the 100-m interferometer, suggest that the background noise level above ~1 Hz is laser frequency noise.

The 1500-m laser strainmeter began operating in August 2016 and has detected a number of seismic waves associated with earthquakes. Figure 6 shows seismic waves from the Fukushima earthquake (Mw 6.9) that occurred at 20:59:49 (UTC) on November 21, 2016. The observed peak-to-peak strain amplitude was 6.4×10^{-7}, which is approximately 20 times larger than typical earth tide amplitudes in this area. Even when the seismic waves passed, no misalignments in the 1500-m optical path were found as a result of the earthquake. The maximum strain rate was $d\varepsilon/dt = 4.8 \times 10^{-7}$/s, which produced a fringe frequency of $(d\varepsilon/dt)(2L/\lambda) = 2.7$ kHz. Using the quadrature interferometer and analysis methods described in the previous section, fringe signals sampled at a rate of 50 kHz ($\gg$2.7 kHz) can be safely used for conversion to strain. This conversion can even be used during the passing of the seismic waves, without any saturation or discontinuity due to cycle slips generally caused by missing fringes.

The initial strain motion shown in the inset to Fig. 6 indicates expansion. Based on the centroid moment tensor (CMT) solution for the earthquake (Global CMT Catalog 2017), the Kamioka site (back azimuth of 256.5°
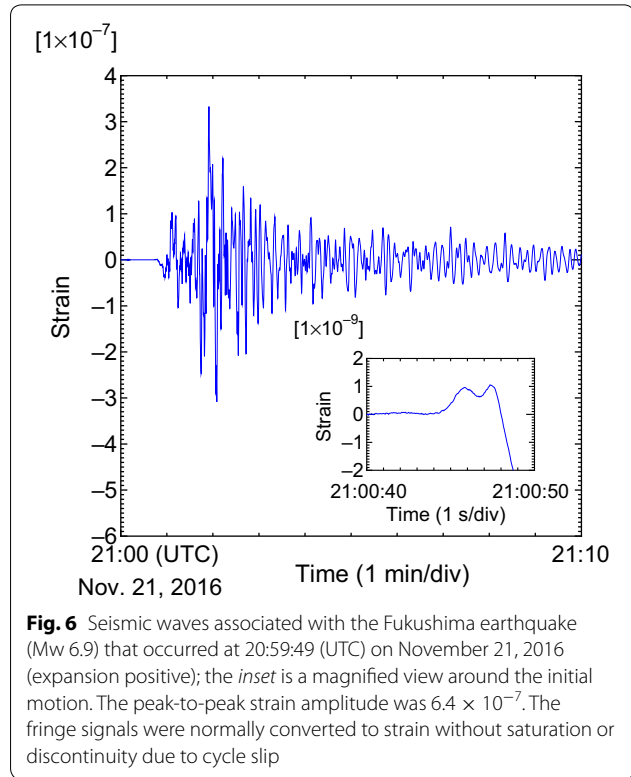
Fig. 6 Seismic waves associated with the Fukushima earthquake (Mw 6.9) that occurred at 20:59:49 (UTC) on November 21, 2016 (expansion positive); the *inset* is a magnified view around the initial motion. The peak-to-peak strain amplitude was 6.4×10^{-7}. The fringe signals were normally converted to strain without saturation or discontinuity due to cycle slip

and distance of 383 km from the epicenter) is likely to be in a compressional field, which is consistent with the sense of the initial strain motion and agrees with the initial pulling motion observed by local seismometers.

Conclusions

A laser strainmeter with a baseline of 1500 m was constructed at an underground site in Kamioka, Japan, and began operating in August 2016. The interferometer mirrors are fixed to the ground with granite blocks in the tunnel housing the KAGRA gravitational wave telescope. All optical paths for the interferometer are housed in a vacuum. A high-frequency-stabilized laser, whose wavelength is locked to an iodine absorption spectrum, is used.

The observed tidal waveform shows reasonable agreement with the theoretical waveform (Fig. 4). The slight difference in amplitude, corresponding to a 13% reduction in the observed waveform, is consistent with topographic effects previously observed for the nearby 100-m strainmeter. Strain spectra from the observed data (Fig. 5) show lower background noise than those obtained from other strainmeters at 2–20 mHz, less than 10^{-12} in the same frequency range. This result suggests that spatial averaging over the long baseline of the strainmeter contributes to noise reduction. Seismic waves up to 6.4×10^{-7} in amplitude were observed without saturation or fringe steps with a signal sample rate of 50 kHz (Fig. 6).

Araya *et al. Earth, Planets and Space* (2017) 69:77

Page 7 of 7

It has been demonstrated that a km-class long-baseline laser strainmeter, without active alignment control, can operate stably and achieve close to design performance. This strainmeter, which has excellent resolution, dynamic range, and bandwidth, provides a new mechanism for observing small ground motion, in particular, at low frequencies on seismic, geodetic, and intermediate timescales.

Author details
[1] Earthquake Research Institute, University of Tokyo, 1-1-1 Yayoi, Bunkyo-ku, Tokyo 113-0032, Japan. [2] Disaster Prevention Research Institute, Kyoto University, Gokasho, Uji, Kyoto 611-0011, Japan. [3] Institute for Cosmic Ray Research, University of Tokyo, 5-1-5, Kashiwanoha, Kashiwa, Chiba 277-8582, Japan.

Publisher's Note
Springer Nature remains neutral with regard to jurisdictional claims in published maps and institutional affiliations.

References
Abe K et al (2013) XMASS detector. Nucl Instrum Methods Phys Res, Sect A 716:78–85

Agnew DC (1986) Strainmeters and tiltmeters. Rev Geophys 24:579–624

Araki T, Enomoto S, Furuno K, Gando Y, Ichimura K et al (2005) Experimental investigation of geologically produced antineutrinos with KamLAND. Nature 436:499–503

Araya A, Kunigi T, Fukao Y, Ymada I, Suda N, Maruyama S, Mio N, Moriwaki S (2002) Iodine-stabilized Nd:YAG laser applied to a long-baseline interferometer for wideband earth strain observations. Rev Sci Instrum 73:2434–2439

Araya A, Morii W, Hayakawa H, Takamori A, Uchiyama T, Ohashi M, Yamada I, Telada S, Takemoto S (2007) Broadband observation with laser strainmeters and a strategy for high resolution long-term strain observation based on quantum standard. J Geod Soc Jpn 53:81–97

Araya A, Takamori A, Morii W, Hayakawa H, Uchiyama T, Ohashi M, Telada S, Takemoto S (2010) Analyses of far-field coseismic crustal deformation observed by a new laser distance measurement system. Geophys J Int 181:127–140

Barnes JA, Chi AR, Cutler LS, Healey DJ, Leeson DB, McGunigal TE, Mullen JA Jr, Smith WL, Sydnor RL, Vessot RFC, Winkler GMR (1971) Characterization of frequency stability. IEEE Trans Instrum Meas 20:105–120

Benioff H (1959) Fused-quartz extensometer for secular, tidal, and seismic strains. Geol Soc Am Bul 70:1019–1032

Berger J, Levine J (1974) The spectrum of earth strain from 10^{-8} Hz to 10^2 Hz. J Geophys Res 79:1210–1214

Berger J, Lovberg R (1970) Earth strain measurements with a laser interferometer. Science 170:296–303

Buklerskii AV, Kart AM, Klyachko BS, Kravchuk VK, Milyukov VK, Melezhnikov IV, Myasnikov AV, Nesterov VV, Rudenko VN (1995) Baksan laser interferometer. Meas Tech USSR 38:1073–1081

Ciddor PE (1996) Refractive index of air: new equations for the visible and near infrared. Appl Opt 35:1566–1573

Crescentini L, Renzella G (1991) A wide-band high-sensitivity laser strainmeter. Rev Sci Instrum 62:1206–1209

Fukuda S, Fukuda Y, Hayakawa T, Ichihara E, Ishitsuka M, Itow Y, Kajita T, Kameda J, Kaneyuki K, Kasuga S et al (2003) The Super-Kamiokande detector. Nucl Instrum Methods Phys Res A 501:418–462

Global CMT Catalog (2017) Global CMT web page. http://www.globalcmt.org/CMTsearch.html. Accessed 16 April 2017. 201611212059A Lat = 37.31, Lon = 141.46, Depth = 12.0, (strike, dip, slip) = (49, 35, −89)/(228, 55, −91)

Heydemann PLM (1981) Determination and correction of quadrature fringe measurement errors in interferometers. Appl Opt 20:3382–3384

Kogelnik H, Li T (1966) Laser beams and resonators. Appl Opt 5:1550–1567

Matsumoto K, Sato T, Takanezawa T, Ooe M (2001) GOTIC2: a program for computation of oceanic tidal loading effect. J Geod Soc Jpn 47:243–248

Mentes G (2010) Quartz tube extensometer for observation of Earth tides and local tectonic deformations at the Sopronbanfalva Geodynamic Observatory, Hungary. Rev Sci Instrum 81:074501. doi:10.1063/1.3470100

Miyoki S, Uchiyama T, Yamamoto K, Ohashi M, Kuroda K, Akutsu T, Kamagasako S, Nakagawa N, Tokunari M, Kasahara K (2006) The CLIO project. Class Quantum Gravity 23:S231–S237

Ohzono M, Sagiya T, Hirahara K, Hashimoto M, Takeuchi A, Hoso Y, Wada Y, Onoue K, Ohya F, Doke R (2011) Strain accumulation process around the Atotsugawa fault system in the Niigata–Kobe Tectonic Zone, central Japan. Geophys J Int 184:977–990

Park J, Amoruso A, Crescentini L, Boschi E (2008) Long-period toroidal Earth free oscillations from the great Sumatra–Andaman earthquake observed by paired laser extensometers in Gran Sasso, Italy. Geophys J Int 173:887–905

Somiya K (2012) Detector configuration of KAGRA–the Japanese cryogenic gravitational-wave detector. Class Quantum Gravity 29:124007. doi:10.1088/0264-9381/29/12/124007

Takemoto S, Araya A, Akamatsu J, Morii W, Momose H, Ohashi M, Kawasaki I, Higashi T, Fukuda Y, Miyoki S et al (2004) A 100 m laser strainmeter system installed in a 1 km deep tunnel at Kamioka, Gifu, Japan. J Geodyn 38:477–488

Takemoto S, Momose H, Araya A, Morii W, Akamatsu J, Ohashi M, Takamori A, Miyoki S, Uchiyama T, Tatsumi D et al (2006) A 100 m laser strainmeter system in the Kamioka Mine, Japan, for precise observations of tidal strains. J Geodyn 41:23–29

Vali V, Bostrom RC (1968) One thousand meter laser interferometer. Rev Sci Instrum 39:1304–1306

Vali V, Krogstad RS, Moss RW (1965) Laser interferometer for earth strain measurements. Rev Sci Instrum 36:1352

Zumberge MA, Berger J, Dzieciuch MA, Parker RL (2004) Resolving quadrature fringes in real time. Appl Opt 43:771–775

Zürn W, Ferreira AMG, Widmer-Schnidrig R, Lentas K, Rivera L, Clévédé E (2015) High-quality lowest-frequency normal mode strain observations at the Black Forest Observatory (SW-Germany) and comparison with horizontal broad-band seismometer data and synthetics. Geophys J Int 203:1787–1803. doi:10.1093/gji/ggv381